Coseismic and post-seismic signatures of the Sumatra 2004 December and 2005 March earthquakes in GRACE satellite gravity

Isabelle Panet, Valentin Mikhailov, Michel Diament, Fred Pollitz, Geoffrey King, Olivier de Viron, Matthias Holschneider, Richard Biancale, Jean-Michel Lemoine

Geophys. J. Int. (2007) **171,** 177–190 doi: 10.1111/j.1365-246X.2007.03525.x

Coseismic and post-seismic signatures of the Sumatra 2004 December and 2005 March earthquakes in GRACE satellite gravity

Isabelle Panet,[1,2] Valentin Mikhailov,[3,4] Michel Diament,[3] Fred Pollitz,[5] Geoffrey King,[6] Olivier de Viron,[3] Matthias Holschneider,[7] Richard Biancale[8] and Jean-Michel Lemoine[8]

[1]*Institut Géographique National, Laboratoire de Recherche en Géodésie, ENSG, 6/8, av. Blaise Pascal, Cité Descartes, Champs/Marne,* 77455 *Marne-la-Vallée Cedex* 2, *France*
[2]*Geographical Survey Institute, Space Geodesy Research Division, 1 Kitasato, Tsukuba, Ibaraki* 305 0811, *Japan. E-mail: panet@gsi.go.jp*
[3]*Institut de Physique du Globe de Paris & University Paris 7-D. Diderot, CNRS,* 4 *place Jussieu,* 75252 *Paris Cedex* 5, *France*
[4]*Institute of Physics of the Earth, Russian Academy of Science, B. Gruzinskaya* 10, *Moscow* 123810, *Russia*
[5]*U.S. Geological Survey, 345 Middlefield road, MS 955, Menlo Park, CA* 94025-3591, *USA*
[6]*Equipe de Tectonique, Institut de Physique du Globe de Paris & University Paris 7-D. Diderot, CNRS, 4 place Jussieu,* 75252 *Paris Cedex* 5, *France*
[7]*University of Potsdam, Department of Applied Mathematics, Am Neuen Palais* 10, D-14469 *Potsdam, Germany*
[8]*Centre National des Etudes Spatiales, Groupe de Recherche en Géodésie Spatiale, 18, Avenue Edouard Belin,* 31401 *Toulouse Cedex* 9, *France*

Accepted 2007 June 14. Received 2007 May 15; in original form 2006 December 6.

SUMMARY

The GRACE satellite mission has been measuring the Earth's gravity field and its temporal variations since 2002 April. Although these variations are mainly due to mass transfer within the geofluid envelops, they also result from mass displacements associated with phenomena including glacial isostatic adjustment and earthquakes. However, these last contributions are difficult to isolate because of the presence of noise and of geofluid signals, and because of GRACE's coarse spatial resolution (>400 km half-wavelength). In this paper, we show that a wavelet analysis on the sphere helps to retrieve earthquake signatures from GRACE geoid products. Using a wavelet analysis of GRACE geoids products, we show that the geoid variations caused by the 2004 December ($M_w = 9.2$) and 2005 March ($M_w = 8.7$) Sumatra earthquakes can be detected. At GRACE resolution, the 2004 December earthquake produced a strong coseismic decrease of the gravity field in the Andaman Sea, followed by relaxation in the area affected by both the Andaman 2004 and the Nias 2005 earthquakes. We find two characteristic timescales for the relaxation, with a fast variation occurring in the vicinity of the Central Andaman ridge. We discuss our coseismic observations in terms of density changes of crustal and upper-mantle rocks, and of the vertical displacements in the Andaman Sea. We interpret the post-seismic signal in terms of the viscoelastic response of the Earth's mantle. The transient component of the relaxation may indicate the presence of hot, viscous material beneath the active Central Andaman Basin.

Key words: earthquakes, geoid, satellite geodesy, subduction zone.

1 INTRODUCTION

The temporal variations of the gravity field reflect the mass redistribution inside the solid Earth and its fluid envelops. In addition to the dominant contribution from solid Earth tides, mass transfers occur at various timescales: daily, semi-annual and annual, interannual, secular, etc. They mainly reflect water redistribution between different reservoirs: the atmosphere, land hydrological systems, oceans and polar ice caps. This phenomenon is responsible for important seasonal gravity variations, reaching a few millimetres of the geoid height at global scale (Dickey *et al.* 1997). Solid Earth processes also cause gravity field variations. Postglacial rebound, reflecting the Earth's response to the last deglaciation, induces geoid variations of a few tenths of millimetres per year. Uplift or subsidence of tectonic origin may also occur. Finally, at shorter time and spatial scales, coseismic redistribution of masses produces local variations of the geoid reaching a few centimetres for the largest events (Dickey *et al.* 1997). Until recently, mapping of temporal variations of the gravity field was restricted to the local scale. This situation has changed after the launch of the GRACE satellite gravity mission in 2002. This mission performs global measurements of the gravity field and its time variations, with an unprecedented high precision and uniform coverage.

The uniform coverage over oceans makes satellite gravity particularly useful for studying earthquakes with epicentres in the oceanic domain such as those occurring in subduction zones. Subduction

zones are indeed the most seismically active areas, affected by the most devastating earthquakes. When an earthquake occurs, the gravity field varies because of mass redistributions resulting from displacement of density interfaces and rock density changes. Consequently, satellite gravity offers a regional view of the event, efficiently complementing the ground based geophysical networks that are often sparse, especially in case of undersea epicentral areas. This is the reason why the new satellite gravity data has been raising interest for earthquake studies (e.g. Gross & Chao 2001). Mikhailov *et al.* (2004) thoroughly investigated the possibility of studying earthquakes using satellite gravity data. Using a statistical signal recognition method, they showed that gravity field variations similar to those caused by Alaska-1964 earthquake should be recognizable in GRACE data at present-day accuracy, and that satellite gravity should allow to discriminate between different fault plane models proposed for the Chile-1960 earthquake. They also showed that the temporal gravity variations associated with the locked areas of the Alaska subduction zone could be recognized from 5 yr of satellite gravity data one order of magnitude more accurate. Sun & Okubo (2004) finally showed that events of 7.5 magnitude could be detected at GRACE expected accuracy.

One of the largest earthquakes of the last century occurred on 2004 December 26 in the Sumatra–Andaman region. It took place west of Northern Sumatra, at the boundary between the subducting Indo-Australian plate and the southeastern part of the Eurasian plate. Besides its unusual size, the Sumatra–Andaman earthquake showed a remarkable complexity, with an initially rapid rupture followed by an important slip propagating northward at decreasing speed (Ammon *et al.* 2005; Banerjee *et al.* 2005; Lay *et al.* 2005; Vigny *et al.* 2005). It was followed by numerous aftershocks, and by a second large earthquake: the Nias 2005 March 28 event (NEIC catalogue).

In the area affected by the 2004 earthquake, the lithosphere of the Andaman Sea overriding plate has undergone complex tectonic deformations during the Neogene—Quaternary, likely resulting in a strong heterogeneity of the crust and underlying mantle (Curray 2005). Formation of the oceanic lithosphere of this backarc basin started 11 Myr ago in the southern part of the Andaman Sea: the Mergui Basin, centred around longitude 97°E and latitude 7°N (see Fig. 1). This first stage of ocean opening stopped 4 Myr ago; then, the spreading centre moved northward and extension was recentred in the Central Andaman Basin, around longitude 94.5°E and longitude 10.5°N (Khan & Chakraborty 2005). This process is still ongoing, and volcanic islands bear witness to the past and present magmatic activity in the Central Andaman Basin and its surroundings.

Han *et al.* (2006) investigated the Sumatra–Andaman earthquake using GRACE K-band microwave ranging satellite-to-satellite tracking data, and explained the important coseismic gravity decrease in the Andaman Sea mostly by the effect of crustal dilatation. In their study, they however compared the predictions of a coseismic model based on the uniform elastic half-space approximation to gravity variations averaged over 6 months after the event, thus including significant post-seismic variations. Our aim in this paper is to refine the analysis of the Sumatra 2004 December earthquake from GRACE geoid models, by providing a better separation and understanding of coseismic and post-seismic contributions, by using a spherical, radially layered Earth's model for coseismic rupture modelling, and by taking into account the lateral heterogeneities of the Andaman Sea lithosphere. We also investigate whether GRACE gravity data are able to bring new insights on the Sumatra 2005 March earthquake.

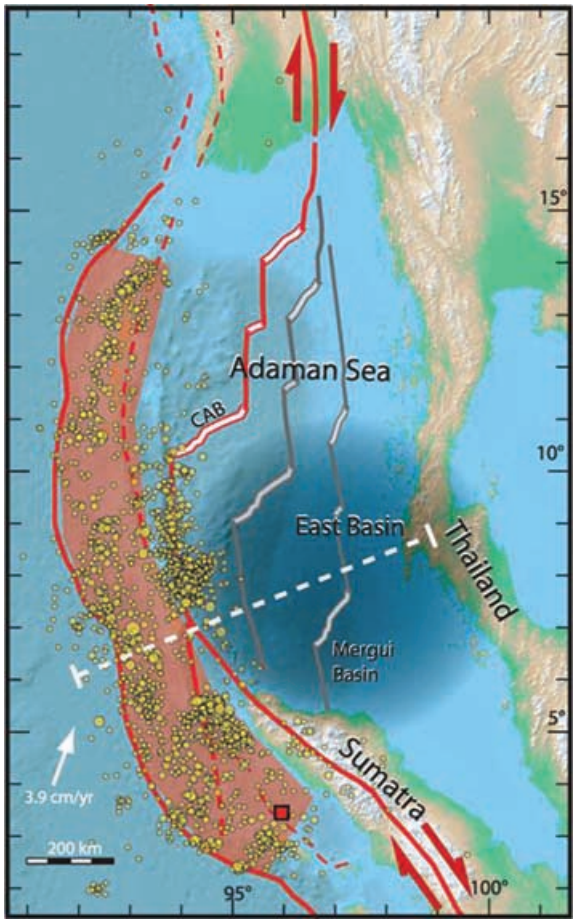

Figure 1. Tectonic map of the area affected by the Sumatra earthquakes. Red square: epicentre of the 2004 December earthquake. Yellow dots: distribution of aftershocks before the 2005 March earthquake. Major active faults are shown in red, older extensional axes are represented in grey (Curray 2005). Strike-slip faults in the north and the south (left arrows) create a region of pull-apart extension. The darkened region corresponds to the coseismic geoid low.

The gravity signal from earthquakes is superimposed on gravity variations of geofluid origin, and GRACE data give an integrated view of all the contributions, contaminated by a noise exceeding the planned mission noise level. Consequently, the earthquake signals are more or less hidden in the data. To extract the earthquake signature more reliably, one has to take advantage of the different characteristics of signal and noise in space and time. This can be done by using a continuous wavelet analysis. Indeed, when applied to temporal gravity data, such analysis allows to unfold the components of the gravity field at different spatial scales and study their time variations separately.

In this paper, we first describe the satellite gravity data that we used and recall the principle of continuous wavelet analysis on the sphere based on the Poisson multipole wavelets. We then present the results of the wavelet analysis of GRACE monthly geoids spanning a period between 2003 January and 2005 September. We then discuss and interpret the coseismic and post-seismic gravity variations evidenced in the wavelet analysis, taking into account the structure and geodynamics of the Andaman subduction zone.

2 GRACE SATELLITE GRAVITY DATA

We use the GRACE geoid anomaly models by Biancale *et al.* (2005), spanning the period between 2002 August and 2005 September. Geoid models are provided in the form of spherical harmonic coefficients up to degree 50, which corresponds to a 400 km resolution (i.e. half-wavelength). The models are computed every 10 days from measurements spanning 30 days, applying a running time average with weight 1.0 for the central 10-day interval, and weight 0.5 for the 10-day intervals before and after it. This allows to reach a finer temporal resolution than the monthly resolution. To avoid amplification of noise at small scales, a smoothness constraint towards EIGEN-GL04S mean gravity field was applied for resolutions smaller than 670 km when computing the geoid solutions from GRACE measurements. Finally, the geoid models are corrected for gravity variations resulting from Earth's, ocean and atmospheric tides and ocean circulation using a barotropic model (Biancale *et al.* 2005). In addition to geodynamic signals and mismodelling errors, the gravity models thus mainly contain hydrology, snow and postglacial rebound contributions, the last two being negligible in the Sumatra area. They also contain noise, mainly consisting of north/south elongated stripes whose position and amplitude vary in time.

We applied additional corrections for hydrological variability. In order to understand the impact of this phenomenon in the Sumatra area, we investigated 10 yr of NCEP and ECMWF hydrological model outputs for soil moisture. These data show that hydrology is characterized by a strong seasonal cycle, with a maximum in summer and a minimum in winter over south Asia. Peak to peak amplitude is about 1 cm of geoid (–5 mm in winter and 5 mm in summer), at 400 km resolution. The influence of hydrology in the area affected by the Sumatra earthquakes is a large-scale spatial trend, with amplitude varying between –1.5 mm in winter and 1.5 mm in summer. We corrected the GRACE geoid models for this contribution using the outputs from the ERA-40 reanalysis of the European Center for Medium-Range Weather Forecast model provided by the MeteoFrance Agency. Even if these corrections reduce the hydrological signal in the GRACE geoids, they do not remove it perfectly. However, as the hydrological signal itself is weak in the area affected by the Sumatra earthquakes, the mismodelling errors should be very small.

The data analysed are the differences between geoid averaged from January to month n of year 2005 and geoid averaged from January to month n of year 2004, with n varying from 1 to 9 ($n = 1$ for January and $n = 9$ for September). Hereafter, we will refer to these data as 'stacked geoid differences'. Comparing the same periods of the year allows the residual annual effects from mismodelled geofluid contributions to be removed efficiently. When increasing the stacking period, one reduces the effect of the noise including stripes, because these components are strongly time dependent and time-averaging cancels them out. On the other hand, by increasing the stacking period (i.e. the time interval under consideration) one progressively enlarges contribution of post-seismic processes. This makes it difficult to isolate precisely the coseismic geoid variation.

Fig. 2 shows the geoid variation observed in GRACE data, at about 400 km resolution, for $n = 1, 4$ and 9. As explained above, they depict difference between 2005 January and 2004 January geoid models ($n = 1$), between averaged over 2005 January–April and averaged over 2004 January–April geoid models ($n = 4$), and between averaged 2005 and 2004 January–September models ($n = 9$). We clearly notice a persistent negative anomaly in the Sumatra area, contaminated by a long wavelength noise probably related to hydrology. To remove this noise and better characterize the geoid variations between years 2004 and 2005, we apply a continuous wavelet analysis.

3 WAVELET ANALYSIS AND RESULTS

3.1 Principle of the continuous wavelet analysis

In this section, we recall the principle of the continuous wavelet analysis. A wavelet is a piecewise continuous function with zero mean and finite energy. It is well localized both in the spatial and in the frequency domains. It is described with two parameters: the position parameter corresponds to the point around which the wavelet concentrates its energy in the spatial domain (its centre), and the scale parameter corresponds to its spatial extent. Wavelets can also be viewed as bandpass filters, with the centre of the bandwidth given by the scale. One may define wavelets on a sphere, provided that the functions satisfy specific admissibility conditions. Such spherical wavelets are useful to study the Earth's gravity field taking into

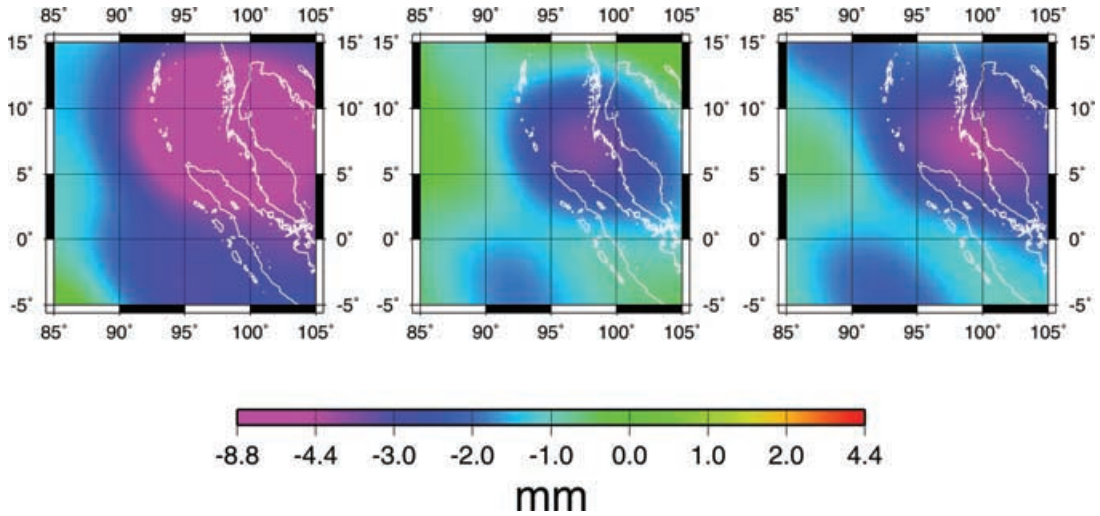

Figure 2. Maps of geoid anomalies in mm over the Sumatra area. Left-hand panel: map of difference between years 2005 and 2004, stacked over 1 month (i.e. 2005 January minus 2004 January). Centre panel: map of difference between years 2005 and 2004, stacked over 4 months. Right-hand panel: map of difference between years 2005 and 2004, stacked over 9 months.

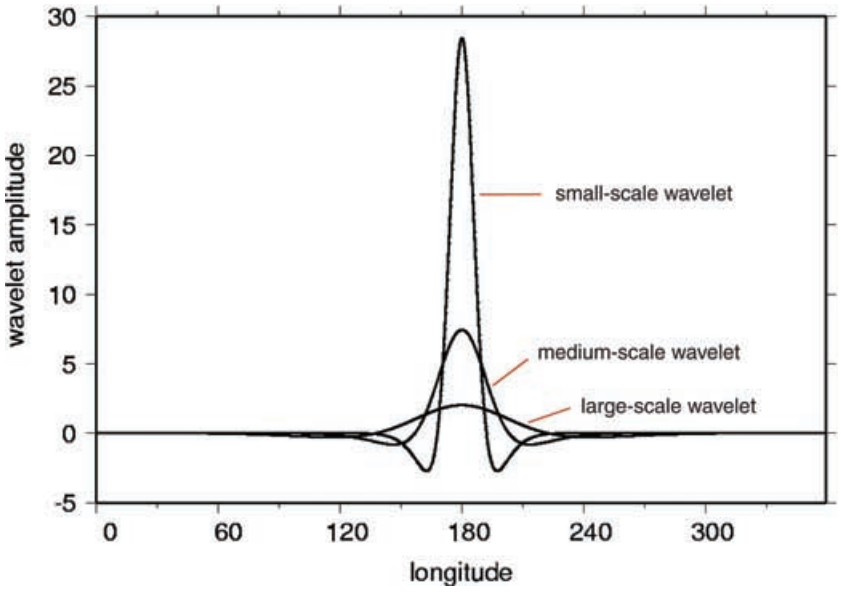

Figure 3. Cross-section of Poisson multipole wavelets of order 3 and scales 5000, 3400 and 2000 km. The wavelets are centred on position (0°N, 180°E) and normalized to unity.

account the Earth's sphericity. Here, we use spherical Poisson multipole wavelets of order 3 that have been introduced in Holschneider *et al.* (2003). To illustrate the signification of the scale and position parameters, Fig. 3 represents a cross-section of those wavelets at three different scales, all located at (0°N, 180°E). Usually a normalization is applied to the wavelets (here their L_2 norm is equal to unity).

Let us denote by g a function in $L_2(S)$, where S is a sphere in R^3 with radius equal to the Earth's radius for instance, and $L_2(S)$ is the space of square integrable functions with respect to S. We note φ_a^e a wavelet of scale a and position e [φ_a^e also belongs to $L_2(S)$]. The continuous wavelet analysis of g is a function of two variables: positions $e \in S$ and scales $a > 0$. It is defined as the family of scalar products $C_{a,e}$:

$$C_{a,e} = \left(\varphi_a^e, g\right). \tag{1}$$

The brackets denote the scalar product on the sphere S, given for x and y in $L_2(S)$ by: $(x, y) = \int_\sigma xy \, d\sigma$. The coefficients $C_{a,e}$ can also be viewed as correlation coefficients between the function g (in our study, the geoid) and the corresponding wavelets. They give a filtered view of function g. From these coefficients, we may exactly reconstruct the function g using a reconstruction formula as explained in Holschneider *et al.* (2003): the set of coefficients $C_{a,e}$ provides an equivalent representation of the function g, unfolding all its components.

When computing the correlation coefficients between the geoid and the wavelets at different scales and positions, we underline the structures in the geoid at the corresponding scales and positions. As the investigated scales and positions vary continuously, this analysis allows to finely characterize the geoid at different spatial scales. Such analysis is particularly helpful when studying composite, non-stationary signals, for which a weak, small-scale component can be masked by a stronger, large-scale contribution and thus may not be detectable by simple eye inspection of the signal. As this weak component will show a good correlation with the small-scale wavelets, it will clearly appear in the analysis at the corresponding wavelet scale. The reader interested in the continuous wavelet transform from a general point of view may refer to the book by Holschneider (1995). Constructions using the Poisson multipole wavelets on the sphere are described in Holschneider *et al.* (2003) and Chambodut *et al.* (2005). An example of continuous wavelet analysis of the gravity potential using such wavelets can be found in Panet *et al.* (2006).

First, we computed the continuous wavelet analysis of the geoid difference between years 2004 and 2005 stacked over 9 months. It contains both the coseismic and post-seismic signals, but due to the long stacking period, it is also less noisy. To investigate more closely the coseismic contribution, we then computed the continuous wavelet analysis of the geoid difference between 2004 January and 2005 January. Finally, to investigate the post-seismic signal, we computed the wavelet analysis of the stacked 2004/2005 geoid differences for various periods of stacking, from 2 to 9 months, after subtracting our previous estimation of the coseismic contribution.

3.2 Results

Fig. 4 shows the wavelet transform of the 9-month stacked geoid difference between years 2005 and 2004, for scales between 2000 and 450 km. We observe very clear anomalies consistent over a wide range of scales. At larger scales, a strong negative anomaly dominates in the Andaman Sea and its surroundings. It is centred at latitude 7°N and longitude 97°E. At smaller scales, this anomaly appears to be precisely located in the Andaman Sea, around the Mergui Basin. A positive anomaly is also observed. It is apparently composed of two parts, the first one centred around latitude 7.5°N and longitude 88°W, and the second one around latitude 0°N and longitude 97°W.

We checked if comparable anomalies were observed before. Fig. 5 shows the 500 km scale wavelet analysis coefficients of the geoid differences between two consecutive years, stacked over the same 9 months period (from January to September). We considered a wide area centred in the Andaman Sea. The left-hand panel represents the difference between 2003 and 2004, illustrating the noise level including contribution from mismodelled geofluid processes at that scale in the area. Note how low the remaining noise level

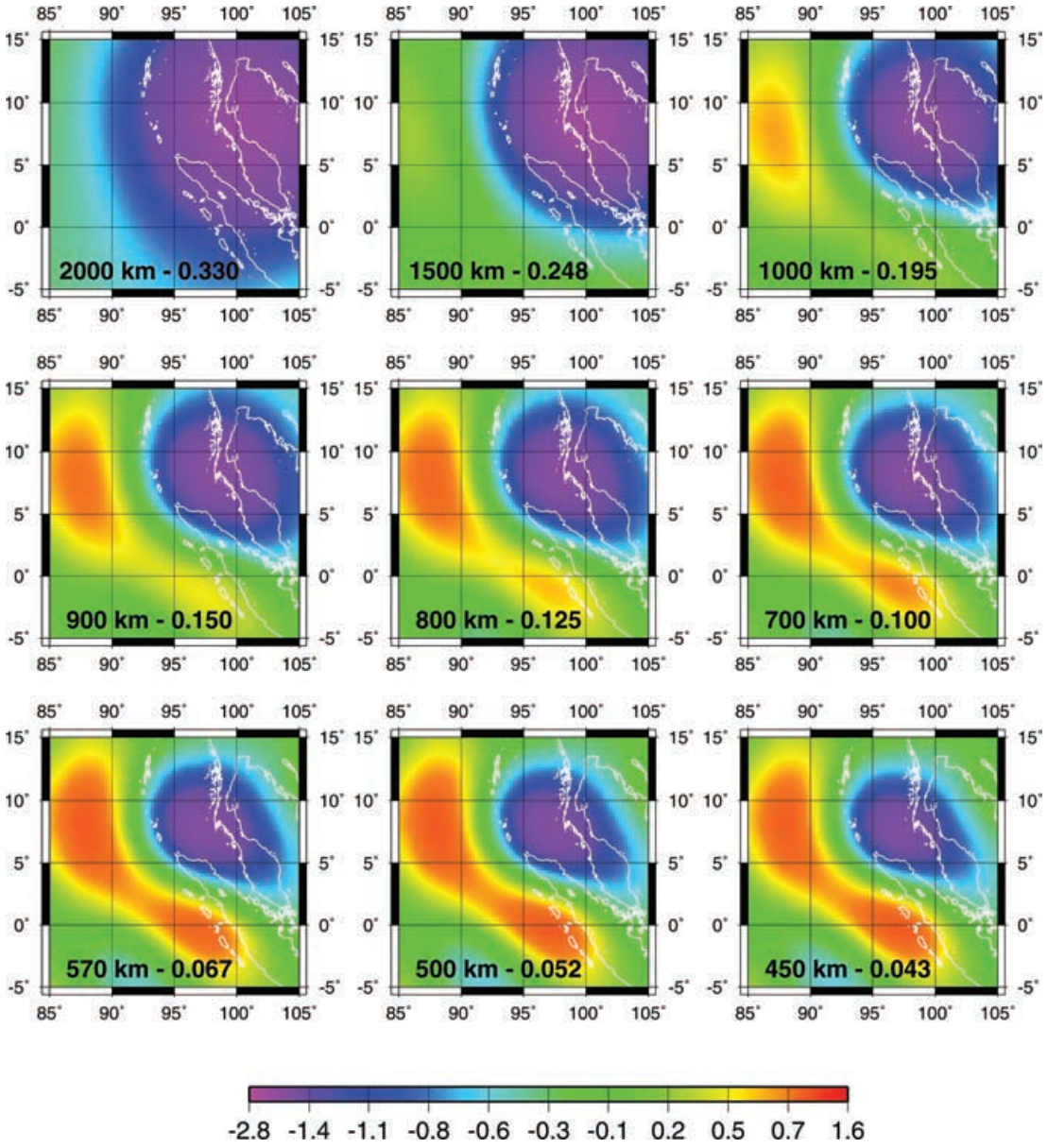

Figure 4. Continuous wavelet analysis coefficients of the geoid difference (mm) between 2005 and 2004, stacked over 9 months. The scale of the analysis is indicated on the subplot, with a scale factor. The colour bar should be multiplied by this scale factor for each subplot.

is. No anomaly is observed in the Andaman Sea. We notice a few anomalies in the north of Australia and in Asia. As they are not stable for consecutive years, we interpret them as residuals of geofluid contributions, probably coming from hydrology. Finally, even if the level of noise seems a little bit higher for the difference between 2005 and 2004 years (right-hand panel), the geoid anomaly that we find in the Sumatra area appears 'at the right time and in the right place' and definitely differs from the noise.

Let us now investigate the time stability of the observed anomalies. Fig. 6 ($n = 1$) represents the 1000 km scale wavelet analysis of the 2005 January minus 2004 January geoid. It is our estimate of the coseismic signal since the contamination with post-seismic effects is the lowest. Fig. 6 ($n = 2$–9) represent the 1000 km scale wavelet analysis of the geoid differences between 2004 and 2005 stacked over n months, minus the coseismic part from Fig. 6, $n = 1$. Fig. 7 is the same as Fig. 6, but at the 570 km analysis scale. First, a comparison of Fig. 4 with Fig. 6 ($n = 1$) and Fig. 7 ($n = 1$) shows that the anomalies are clearly persistent over 9 months, in their general features. Second, we evidence a time variation of the gravity signal, which consists of a slow reduction of the strong negative anomaly. A stabilization of the signal occurs after 4 months at the 570 km scale (Fig. 7, $n = 5$–9), whereas the large-scale components continue to decrease (Fig. 6, $n = 5$–9). For stacking periods larger than 4 months, we detect at 570 km scale a slight persistent anomaly that we associate with the Nias earthquake. This anomaly is made of a relatively small maximum over latitude 2°S, longitude 97°E (at the earthquake epicentre), and a relatively small minimum over latitude 4°N, longitude 104°E, present on all plots from Fig. 7, $n = 4$–9. It again appears 'at the right time and in the right place', and its smaller amplitude corresponds to the smaller magnitude of the seismic event. A close-up is presented on Fig. 8 and clearly shows the persistence of the anomaly. Finally, Fig. 9 shows the time variation of the maximum value of the wavelet coefficients at 1000 and 570 km scales for increasing stacking periods, after subtracting the

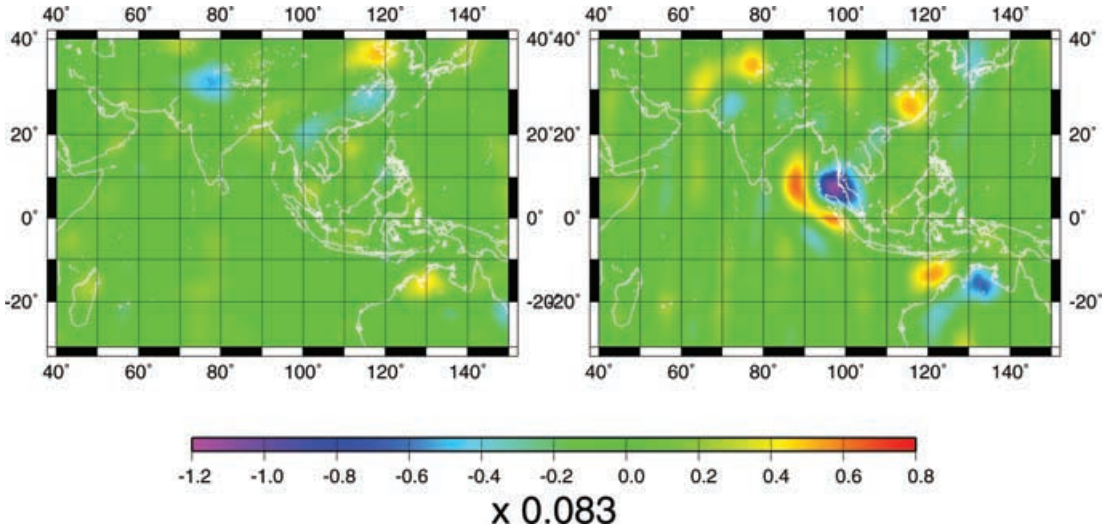

Figure 5. Continuous wavelet analysis coefficients at 500 km scale of the geoid difference (mm) between 2005 and 2004, stacked over 9 months (right-hand panel), and of the geoid difference between 2004 and 2003, stacked over 9 months (left-hand panel).

coseismic part $n = 1$ (left-hand panel). It also shows the time evolution of the spatially averaged wavelet coefficients (right-hand panel). As mentioned previously, both figures show a clear change in the trends for the two spatial scales approximately 3 months after the December event, with further stabilization of the amplitude of the 570 km scale wavelet coefficients after 4 months. The close correlation of the time variations of the maximum amplitude of the wavelet coefficients with their spatially averaged values demonstrates the stability of the mentioned features. Such behaviour was also observed using a different approach by Lemoine *et al.* (2007).

It is worth noting that the noise mainly presented as time-varying 'stripes' is not likely to produce such slow, localized variations in the Andaman area. The unmodelled hydrology processes cannot produce such a large signal centred over oceanic areas. The gravity effect of the ocean has been removed using the barotropic MOG2D ocean model by Carrere & Lyard (2003). In addition, it does not seem very likely that the Sumatra–Andaman earthquake could create such a slowly decaying, localized oceanic current. We however investigated 4 yr of AVISO sea level anomalies from the Topex-Poseidon and Jason satellite altimetry missions, spanning 2002 January to 2006 May, and did not find any particular anomaly in the Andaman Sea.

Thus, we conclude that the anomalies we find are of geodynamic origin. The negative anomaly is clearly caused by the 2004 December earthquake. A slow gravity relaxation at two characteristic timescales occurs in the following months. We also detected a signal linked with the 2005 March earthquake.

4 DISCUSSION

We now discuss the geodynamic implications of the observed coseismic and post-seismic gravity signals associated to the Sumatra earthquakes.

4.1 Gravity variations caused by an earthquake

Gravity field variations caused by an earthquake can be separated into two components. The first component is the gravity effect associated with displacement of density interfaces. The main density interface is at the Earth surface or at the ocean bottom, but the Moho interface should also be considered. The effect of relatively thin sedimentary layers is negligible. The second component of the total gravity variation is the effect caused by changes of the density as a result of deformation hereafter called dilatation (we use this term in its broad sense including both decompaction under extension and compaction under compression). In addition to the size and depth of the fault plane, and the amount of slip, the gravity effect of dilatation mainly depends on the fault plane's dip and the compressibility of rocks as given by the Poisson ratio.

When analysing surface data, the measured gravity variations appear to be very close to the gravity effect from the Earth's surface displacement (e.g. Barnes 1997). However, in satellite gravity data such as GRACE geoids, the intense short wavelength anomalies caused by movements of the density interfaces are considerably smoothed. The gravity variations caused by dilatation of the crustal and mantle rocks can no longer be neglected, especially for large earthquakes (Han *et al.* 2006). Extension predominates in the superficial layers whereas compression prevails at depth, in the mantle. For a subduction earthquake, dilatation mainly produces at long wavelengths a gravity decrease above the forearc and backarc basins whereas the total gravity signature of both surface and Moho displacements at large scales is mainly a gravity increase in the forearc region and above the fault planes.

4.2 2005 March earthquake

The 2005 March earthquake is a 'smaller' event and its detection on Fig. 8 shows that using wavelets, it is possible to detect earthquakes with a magnitude as 'low' as 8.7 with the present-day accuracy of GRACE data—even if the associated coseismic gravity changes were observed close to the limit of our detection possibilities, at the smallest wavelet scales. The presence of a notable negative lobe suggests that rock dilatation is also important for this earthquake. At larger scale, Fig. 6, $n = 5$–9 show that the area affected by the Nias earthquake likely undergoes a large scale relaxation that seems to be the southward propagation of Andaman earthquake relaxation area, discussed below. Contrary to the case of the Andaman earthquake, we do not observe any reduction of the coseismic negative anomaly for increasing stacking periods for the Nias earthquake: the

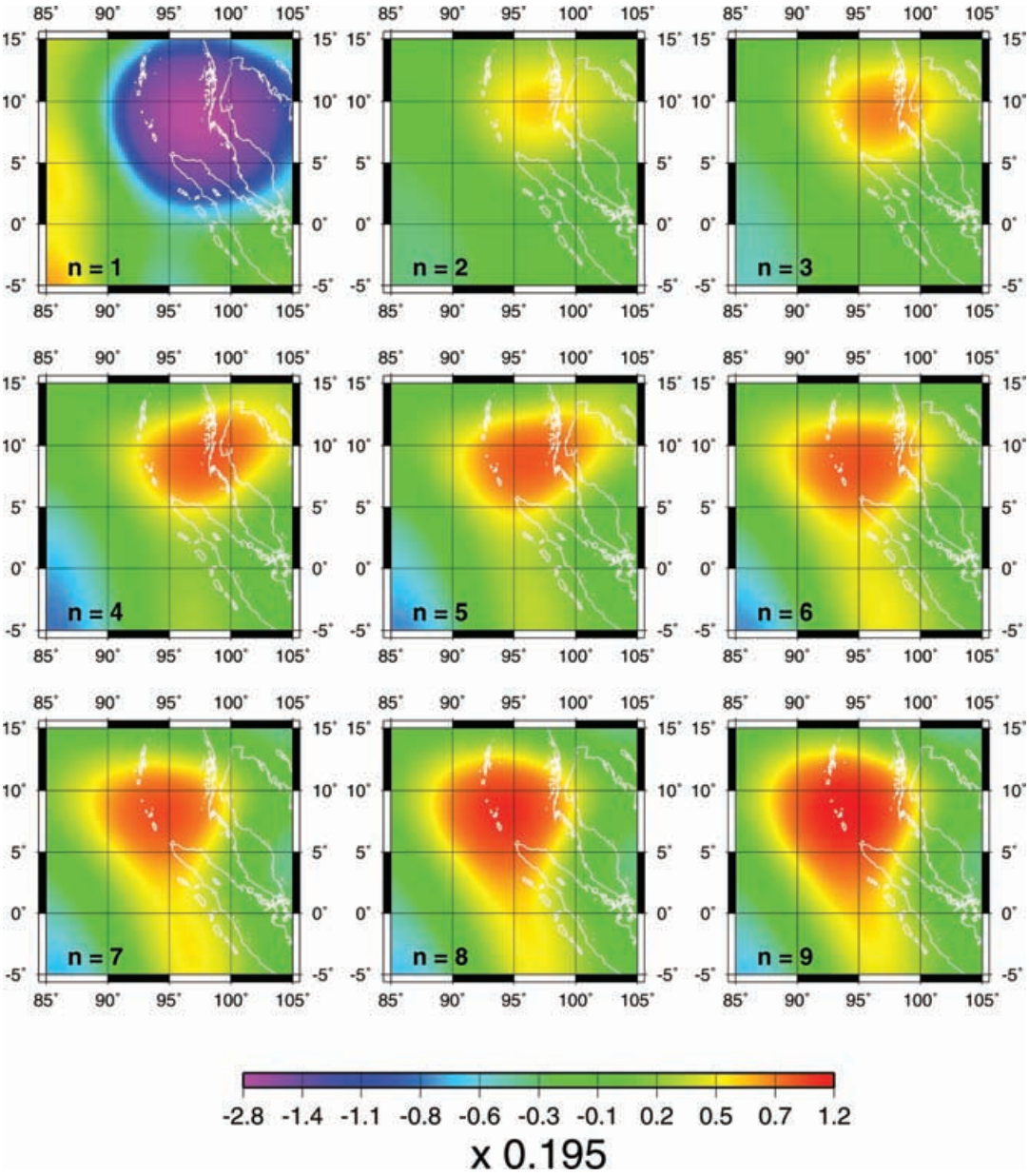

Figure 6. Continuous wavelet analysis coefficients at 1000 km scale of the geoid 2005/2004 differences (mm) stacked over *n* months, with *n* between 1 and 9, illustrating the time variation of the gravity geodynamic signal. On the upper left subplot, the coseismic signal ($n = 1$: January 2005–January 2004) is represented. It has been subtracted from the other subplots ($n = 2$–9). The value of *n* is indicated on each subplot. Note stable growth of the signal with stacking interval (i.e. with time).

coseismic anomaly rather tends to be amplified. This results from the increasing weight of the coseismic variation when the stacking period increases, but this might also suggest different processes in the post-seismic regime for these two earthquakes.

4.3 2004 December earthquake: coseismic signal

To compute the synthetic geoid effect of the 2004 December earthquake, we used the model of rupture along fault planes by Banerjee *et al.* (2005). In this model, parameters of the fault planes are estimated from geodetic and seismology data. To the difference with the fault planes model used in Han *et al.* (2006) study, the slip is uniform on each fault plane, and the dip of the planes is greater. As the GPS measurements of surface displacements that constrain the model span a period of a few weeks, the rupture model also accounts for part of the post-seismic slip. We computed both displacements at density interfaces and variations of density (dilatation) using the source response functions by Pollitz (1996) in an elastic, compressible and layered spherical self-gravitating Earth. The elastic stratification of the model is based on the PREM model (Dziewonski & Anderson 1981). Each layer is homogeneous. The interface displacements and density variations can be directly converted into loads at different depths, from which we compute the geoid variation according to Wahr *et al.* (1998). The approach is also explained in Mikhailov *et al.* (2004). Finally, let us underline that, for an earthquake of the magnitude and size of the 2004 December event, the half-space approximation used by Han *et al.* (2006) may

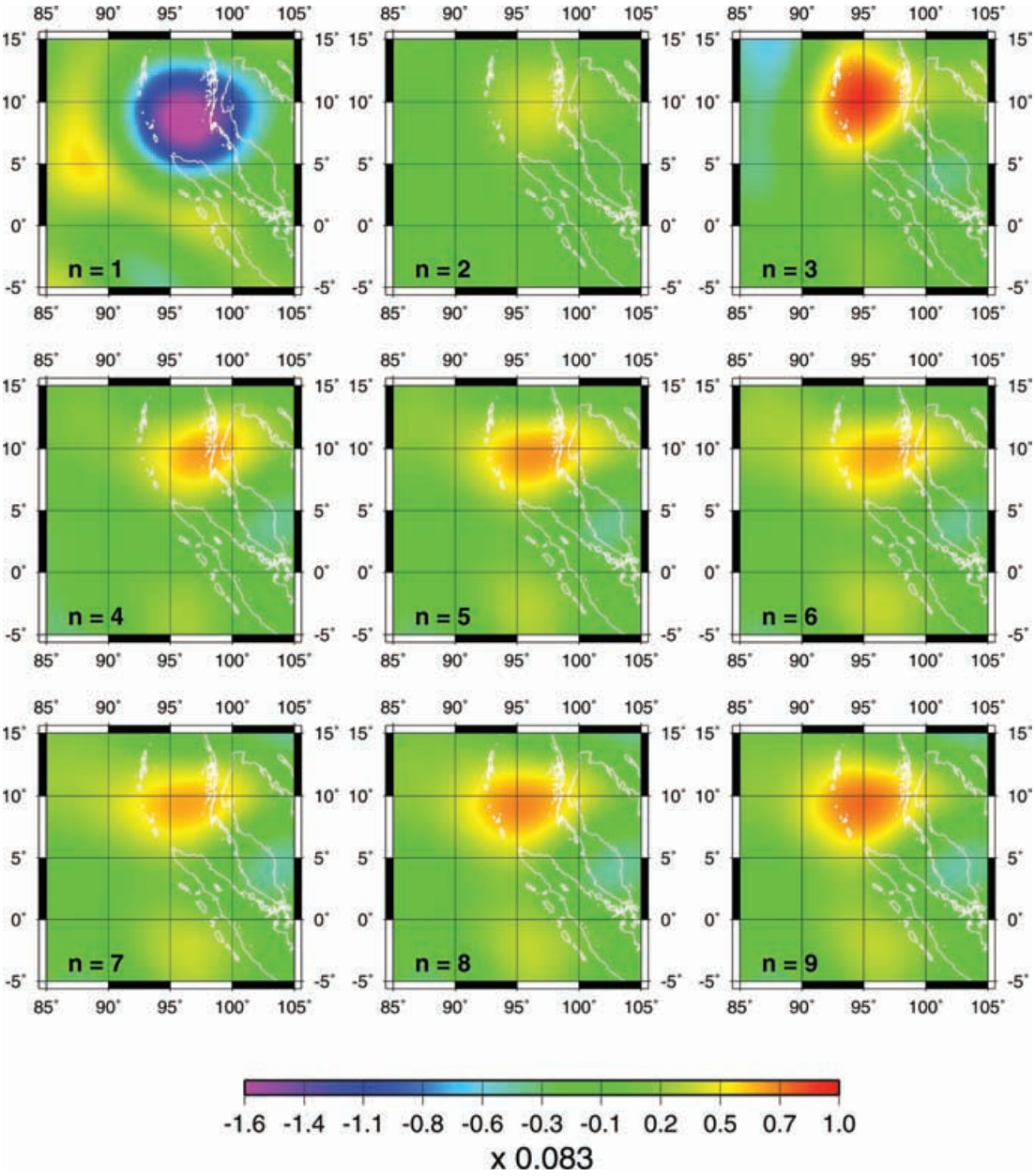

Figure 7. Continuous wavelet analysis coefficients at 570 km scale of the geoid 2005/2004 differences (mm) stacked over *n* months, with *n* between 1 and 9, illustrating the time variation of the gravity geodynamic signal. On the upper left subplot, the coseismic signal ($n = 1$: January 2005–January 2004) is represented. It has been subtracted from the other subplots ($n = 2$–9). The value of *n* is indicated on each subplot.

not be accurate enough (Banerjee *et al.* 2005). Indeed, for a ruptured area exceeding 1200 km, one may expect the lower mantle to be affected by the earthquake, and the response of the whole Earth to the coseismic stress should be computed, introducing a radial stratification of the model.

The comparison between the geoid anomaly predicted by the model and the observations can be done in terms of the coefficients of their wavelet analysis. We considered a wide range of wavelet scales for scales larger than 620 km. Indeed, because of the regularization applied at high harmonics degrees only when computing the geoid solutions from GRACE measurements, not only the noise but also the signal in the data may have been attenuated at the corresponding scales. This constraint starts to act at spherical harmonic degree 27 (resolution about 740 km), but it becomes important above degree 33 (resolution about 610 km). Therefore, a quantitative amplitude comparison with a model may be misleading at too small scales. It is why we use the smallest scales of the wavelet analysis of GRACE geoids only for a qualitative characterization of the signal. On the other hand, comparisons between constrained and unconstrained geoid solutions show that the stabilization procedure applied in the computation of the CNES geoids does not deteriorate the gravity signal for spherical harmonics degrees lower than 27–30 (Lemoine *et al.* 2007). Figs 10(a, c) and 11(a, c) thus show the results for wavelet scales 1000 and 620 km. Note that the geoid anomalies evidenced in the 620 km scale wavelet analysis may be, already, slightly attenuated in result of the applied constraint. First, the wavelet analysis of the synthetic signal reproduces the negative anomaly over the Andaman Sea, but the amplitude of the predicted

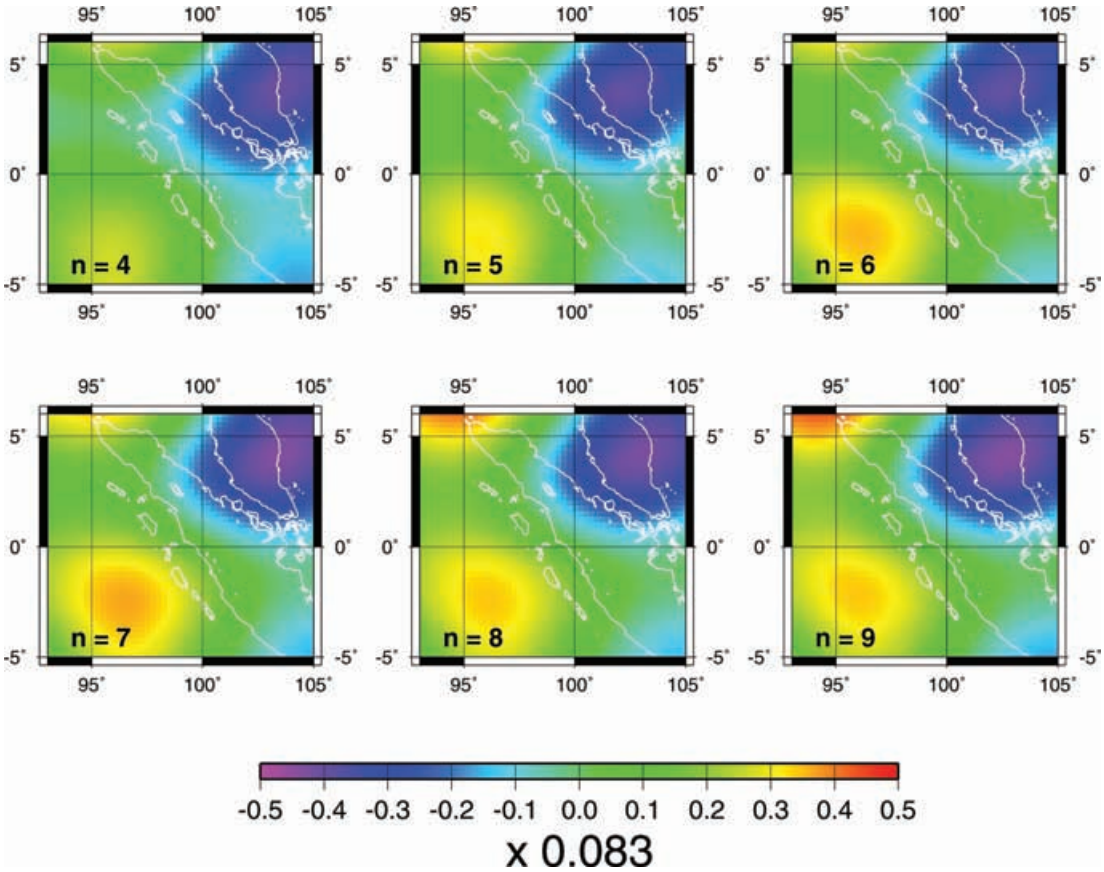

Figure 8. Zoom around the area affected by the Nias earthquake, from Fig. 7.

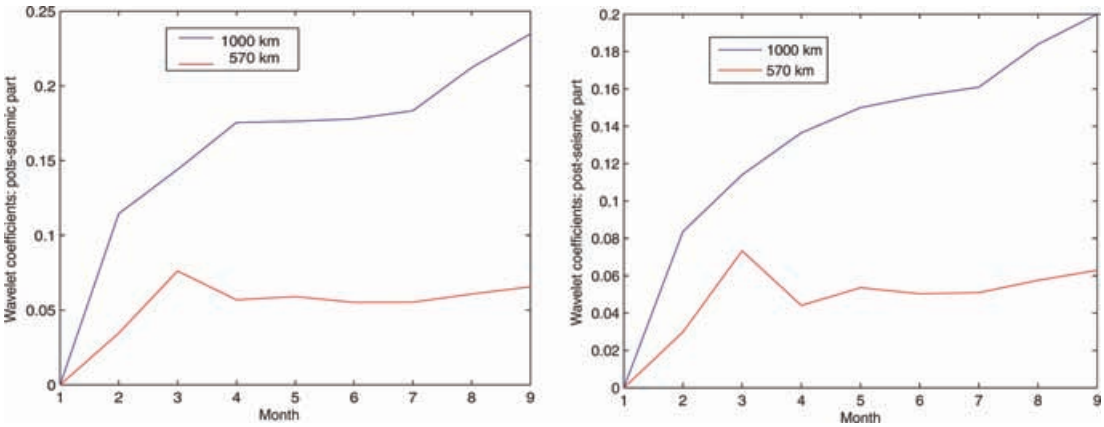

Figure 9. Left-hand panel: time variation of the maximum value of the wavelet coefficients for different stacking intervals n from Fig. 6 (1000 km scale) and Fig. 7 (570 km scale) relative to $n = 1$. Abscissa axis depicts the stacking period ($n = 1$–9, same as in Figs 6 and 7). Right-hand panel: time variation of the value of the wavelet coefficients from Fig. 6 (1000 km scale), averaged over the area between 93°E–98°E in longitude and 5°N–10°N in latitude, and the same for the wavelet coefficients from Fig. 7 (570 km scale), averaged over the area between 94°E–96°E in longitude and 9°N–11°N in latitude. As for plot A, variation is shown relative to $n = 1$.

negative anomaly is much smaller than the observed one. Second, the observed positive anomaly associated with the 2004 December earthquake (Fig. 11) is weaker than what the model predicts, and centred more northward.

As a first refinement of our elastic model, we introduce heterogeneity in the lithosphere of the overriding plate. According to Curray (2005), the Andaman Sea lithosphere is strongly inhomogeneous. It comprises a large number of ridges and basins. Numerous thrusts are documented by seismic profiles, many of them proved to be presently active. In result of the coseismic stress changes, extension occurs in the overriding plate, including the Andaman Sea area. Given the tectonic characteristics of this area, it is likely to deform more than a model involving a homogeneous lithosphere predicts. To more precisely quantify the response of the Andaman Sea lithosphere to extensional stresses, we developed a 2-D model of extension of an inhomogeneous, compressible elastic layer (see

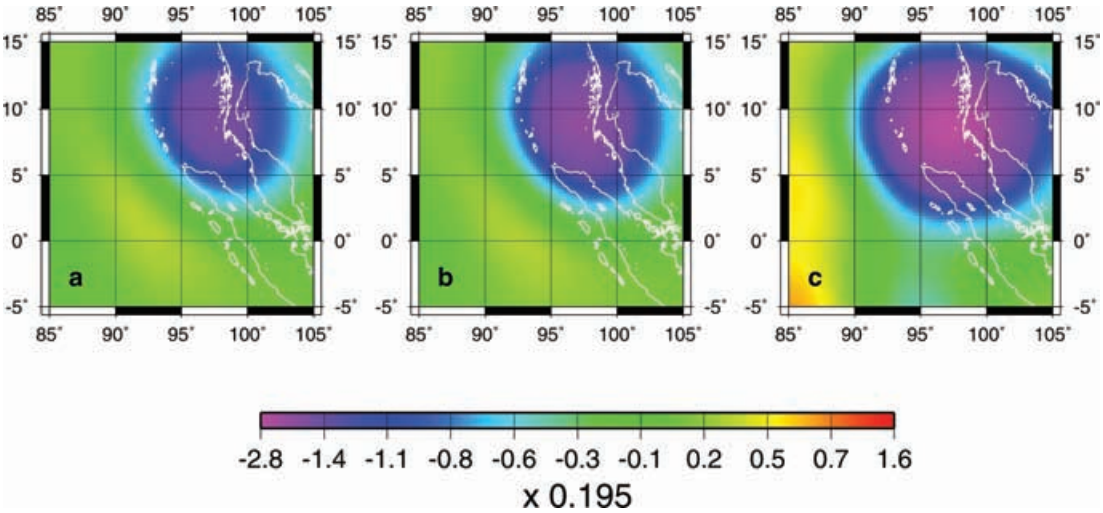

Figure 10. Continuous wavelet analysis coefficients at 1000 km scale of the geoid anomaly (mm) resulting from Banerjee *et al.* (2005) model of the Andaman 2004 December earthquake. A self-gravitating, spherically layered, compressible Earth model is used (subplot a). On subplot (b), we added the effect of 15 cm of subsidence in the Andaman Sea to the model. Subplot (c): coefficients of the wavelet analysis of GRACE geoid difference between January 2004 and January 2005.

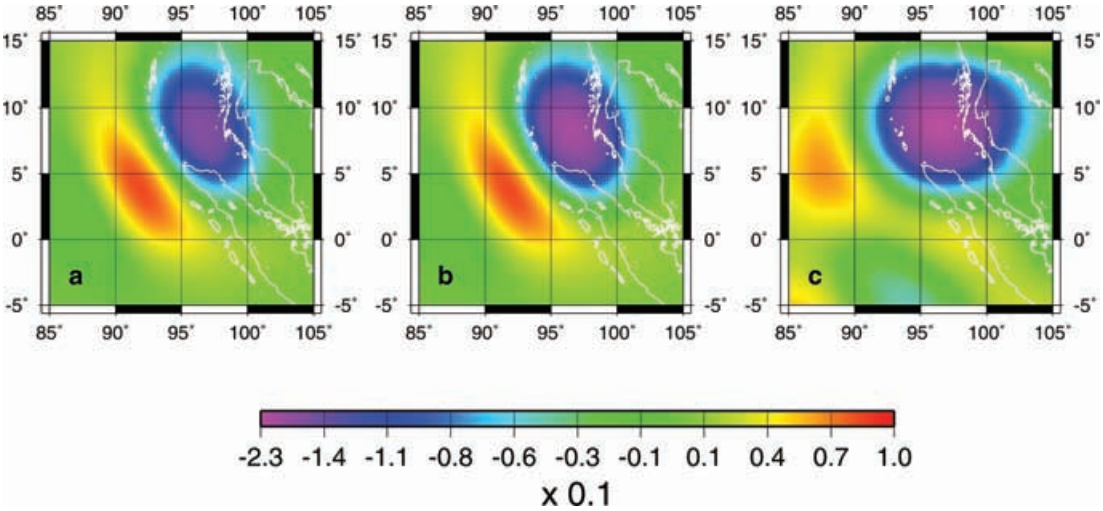

Figure 11. Same as Fig. 10, but the scale of the analysis is 620 km instead of 1000 km.

Appendix A). We assume that during the 2004 December event, the western limit of overriding Andaman Sea plate moved of about 5 m westward. Models of dislocation in a homogeneous elastic medium suggest that about half of this movement was accommodated in the vicinity of the trench. About 2.5 m of remaining westward displacement would thus be accommodated through extension in the area between the vicinity of the trench and the Thailand peninsula considered to be fixed (Vigny *et al.* 2005; Hashimoto *et al.* 2006). Heterogeneity of the Andaman Sea lithosphere was modelled by blocks with different compliances. Introduction of such heterogeneity and the applied external stresses producing 2.5 m extension yield additional 15 cm seafloor subsidence in the most compliant the Andaman Sea block. It would produce an additional coseismic negative anomaly in the Andaman Sea. Figs 10b and 11b show the geoid anomalies predicted when adding 15 cm of subsidence in the Andaman Sea to our previous laterally homogeneous model. The fit with the observations has been clearly improved. It might even be possible to consider larger amounts of subsidence.

Finally, the small amplitude of the observed positive lobe could indicate a stronger crustal dilatation, or less compressibility of the mantle than predicted by the numerical model. In any case, because of its small amplitude, the positive lobe in the data might be blurred by remaining noise and this could affect its shape and location. This small amplitude may also result from an attenuation of the signal in the used geoids that is likely to occur at spherical harmonics degrees larger than 27, indicating that the coseismic positive variation is a smaller scale feature than the negative one. Indeed, applying a high-pass filter to the geoids reveals more clearly a small-scale positive geoid variation in the area where it should occur based on the models predictions. However, its detection is really at the limits of GRACE capabilities, thus the main feature, at GRACE resolution, remains a strong geoid low in the Andaman Sea.

4.4 2004 December earthquake: post-seismic signal

Large interplate earthquakes often cause significant post-seismic deformations. Here, we note a clear relaxation of the geoid anomaly

associated with the Sumatra events, with three main features. First, we find two characteristic timescales. A transient signal occurred in the Andaman Sea at 570 km scale, and stabilized within 3–4 months. Fig. 7 shows that it is localized slightly northward of the area of maximum coseismic subsidence. It is superimposed on a broader, slowly relaxing signal still evolving after 9 months. Relaxation of the gravity signal began in the Andaman Sea and spread around the trench and finally southward, to the area affected by the 2005 March earthquake (Fig. 6). The second main feature is that this relaxation corresponds to an increase of the gravity field over broad areas (this corresponds to a decrease of the negative anomaly that appeared during the earthquake). Last, we note that the area affected by gravity relaxation only partly coincides with the area of high aftershock activity. The Andaman Sea, that exhibits a strong coseismic gravity variation, concentrates a large part of the post-seismic variations.

The fact that the area of small-scale post-seismic gravity variations intersects the area of high aftershock activity (see Fig. 7, for $n = 3$ months of stacking), and that these gravity variations take place at the same time as the aftershocks, suggests that the fast component of the gravity field relaxation may be at least partly related to stress release in the lithosphere. However, the initiation of the relaxation rather far from the trench (see Figs 6 and 7 for $n = 2$) and its slow-varying component, suggest that several processes may contribute to the observed gravity changes. Let us now discuss possible explanations.

Post-seismic deformations may be caused by afterslip, poroelastic effects, or by the viscoelastic response of the crust and mantle to the coseismic stress changes. Poroelasticity alone is not likely to explain our observations since this phenomenon produces much more localized effects (Masterlark *et al.* 2001). Afterslip probably occurred at depth in the months following the earthquake given the large number of registered aftershocks and the large amount of post-seismic slip registered by regional geodesy (Subarya *et al.* 2006; Banerjee *et al.* 2007). Hashimoto *et al.* (2006) showed that, for the Sumatra 2004 and 2005 earthquakes, the GPS measurements of the post-seismic horizontal velocities can be explained well by an afterslip model. The fault planes of their post-seismic model have the same orientation as those of their coseismic model but extend deeper. In their model, the post-seismic slip along the fault planes occurs roughly in the same direction as the coseismic slip during the first 3 months following the 2004 December earthquake. As a consequence, post-seismic uplift should be expected in the area above the fault planes (which roughly corresponds to the area affected by the aftershocks), and subsidence should occur eastward of the fault planes. If positive gravity changes may thus be expected around the aftershocks area, such a model is not likely to produce the observed gravity increase in the whole Andaman area. Consequently, afterslip (if any) must be superimposed on another process to explain the gravity changes.

Coseismic models show that the rock compressibility should be taken into account to reproduce GRACE coseismic observations (Han *et al.* 2006). When considering the response of deep layers, the viscosity can no longer be neglected. The Sumatra 2004 and 2005 earthquakes indeed generated large coseismic stress variations in a region of about 1000 km both laterally and vertically around the faults (Pollitz *et al.* 2006). The upper and top of the lower mantle must have been affected by the stress changes. The fact that the relaxation observed in Figs 6 and 7 is a large-scale phenomenon (reaching the area affected by the Nias earthquake) suggests a mechanisms acting at depth in the mantle. Moreover, it is significant that both the fast and slow relaxation components start in the Andaman Sea, in the vicinity of the Central Andaman Basin. Indeed, the Andaman Sea may be opening in this area and consequently, viscous material may be present at depth. All these observations indicate that viscous deformations could explain better a part of the gravity variations.

Usually, viscoelastic relaxation in the mantle is expected to produce slow deformation, over a few years or decades, under an assumption of a linear rheology, whereas the fast relaxation is attributed to afterslip on the faults. However, ductile olivine exhibits a non-linear rheology, which is likely to cause transient viscoelastic deformations after an earthquake (Minster & Anderson 1981; Karato & Wu 1993). Such deformations may be accounted for using a linear rheology model with a low viscosity. Pollitz *et al.* (2001) and Pollitz (2003) thus showed that a vigorous mantle flow beneath a fault could explain the fast crustal deformations after the 1999 Hector Mine earthquake, in the opposite direction with respect to the direction that an afterslip model predicts. A viscosity of the order of 10^{17} Pa s was inferred for the upper mantle right after the earthquake. The mantle viscosity was actually lowered by the large coseismic stress step, and then gradually increased with time to converge around 10^{19} Pa s after a few years of relaxation. A transient rheology was also invoked by Ivins (1996) to explain the fast post-seismic deformations after the 1992 Landers earthquake, and interpreted in the framework of composite media theory. Such media are made of a harder matrice with softer inclusions. They are characterized by a bi-viscous rheology, with a short-term viscosity causing a fast relaxation and a long-term viscosity causing slower post-seismic signals (Ivins 1996). The fast relaxation is due to the easier deformation of the soft inclusions whereas the slower one reflects the response of the matrice.

Our observations are consistent with a bi-viscous rheology model. They may indicate the presence of less viscous, hot material under the Central Andaman Basin, with possible non-linear rheology. The asthenosphere below active spreading rifts is indeed shallower and hotter. Moreover, volcanic activity during year 2005, triggered by the 2004 December earthquake, was reported by Mishra *et al.* (2007) in the previously dormant Narcondam volcanic zone (lon. 94°E, lat. 14°N), and in the Barren volcano area (lon. 93.7°, lat. 12°N). The authors thus suggest that magma displacements occurred at depth, which is consistent with our hypothesis. Finally, we note that a bi-viscous rheology is also consistent with post-seismic deformation modelling for the Sumatra–Andaman earthquake by Pollitz *et al.* (2006). They indeed showed that a viscoelastic model involving a bi-viscous rheology in the asthenosphere may explain the GPS measurements of horizontal post-seismic displacement as well as an afterslip model. The relaxation characteristic timescale is inversely proportional to the viscosity of a layer. Relaxation over a few months as observed at the 570 km scale could indicate the presence of material with viscosities of the order of 10^{17} Pa s below the Central Andaman ridge. Comparable values have also been proposed in the literature in the case of oceanic asthenosphere (Pollitz *et al.* 1998).

The viscoelastic model of Pollitz *et al.* (2006) predicts a pattern of vertical post-seismic displacements involving uplift at a rate of 8–10 cm yr^{-1} around the trench, and subsidence at the same rate in a large part of the Andaman Sea area. To compare with, GPS measurements evidenced post-seismic uplift in Port Blair (lat. 11.6°N; lon. 92.7°E), where coseismic subsidence was registered (Galahaut *et al*. 2006; Banerjee *et al*. 2007), but vertical movements are more difficult to assess at Phuket (Hashimoto *et al*. 2006). However, the model developed by Pollitz *et al.* (2006) does not take into account the lateral structure of the crust and mantle. The subducting slab imposes a clear limitation to mantle flows, and different viscosi-

ties may be considered in the oceanic and continental mantle. Introducing such structuration in a viscoelastic model permitted Hu *et al.* (2004) to explain successfully the post-seismic uplift observed in the areas undergoing coseismic subsidence after the Chile 1960 earthquake. Tide gauge measurements indeed showed 75 cm of total uplift in the coseismic subsidence area during the 29 yr following the Chile 1960 earthquake, with probably higher uplift rates during the first years after the earthquake (Hu *et al.* 2004). The overriding slab tends to move westward, in the direction of the trench, but, because the underlying westward mantle flow is stopped by the subducting slab, it becomes oblique and generates a vertical, uplift component; the larger the viscosity contrast between oceanic and continental mantle, the faster and larger the uplift. This difference of viscosities plays a role on the vertical movements but does not change greatly the horizontal post-seismic velocities. In the case of the Sumatra–Andaman subduction, the viscosity contrast could be important and generate uplift in the Andaman Sea.

5 CONCLUSION

By applying a wavelet analysis to the GRACE geoids, we provide evidence for clear gravity signals associated with the Sumatra 2004 and 2005 earthquakes. A strong gravity decrease occurred in the Andaman Sea after the 2004 December earthquake. It was followed by a fast gravity increase again localized in Andaman Sea and superimposed on a slower and broader increase of gravity reaching the trench and the area affected by the Nias earthquake. The wavelet analysis allowed us to separate the different components of relaxation, and to localize the coseismic gravity low in the Andaman Sea. To explain fully these observations, it is necessary to take into account the specific structure of the Andaman Sea lithosphere and the asthenosphere. Additional coseismic subsidence is likely to have occurred in the Mergui Basin as a result of the overriding plate lithospheric heterogeneity, providing a better fit of the gravity observations. The fast relaxation component may be caused by the response of a highly viscous material under the active Central Andaman Basin, and may be also partly related to afterslip manifested by the aftershocks activity. Further work has to be carried out in order to reach a more complete understanding of the gravity variations and how they relate the 2004 December and 2005 March events. These observations underline the importance of the viscous response of the Earth to the earthquake stresses and show that GRACE can be used to monitor post-seismic deformation. Such direct observations of the post-seismic relaxation show the wide perspectives opened by satellite gravimetry for understanding and monitoring the seismic cycle. Ongoing and future satellite gravity missions should thus contribute to a more accurate view of the Earth's rheology.

ACKNOWLEDGMENTS

We used the altimeter products produced by Ssalto/Duacs and distributed by Aviso, with support from CNES. This study was supported by CNES (TOSCA science committee) and through the SAGER: Sumatra-Andaman Great Earthquake Research, ANR-05-CATT-12. All maps were plotted using GMT software (Wessel & Smith 1995). We thank I. Velicogna, J. Wahr, C.K. Shum and an anonymous reviewer for their careful readings that contributed to improve our manuscript. This is IPGP contribution number 2243.

REFERENCES

Ammon, C. *et al.*, 2005. Rupture process of the 2004 Sumatra-Andaman earthquake, *Science*, **308,** 1133–1139.

Banerjee, P., Pollitz, F. & Bürgmann, R., 2005. Size and duration of the great 2004 Sumatra-Andaman earthquake from far-field static offsets, *Science*, **308,** 1769–1772.

Banerjee, P., Pollitz, F., Nagarajan, B. & Burgmann, R., 2007. Co-seismic slip distribution of the 26 December 2004 Sumatra-Andaman and 28 March 2005 Nias earthquakes from GPS static offsets, *Bull. Seismol. Soc. Am.*, **97**(1A), S86–S102.

Barnes, D.F., 1997. Gravity changes during the 26 years following the 1964 Alaskan earthquake, in *Geological Studies in Alaska, USGS Professional Paper,* **1614**, 115–122.

Biancale R., Lemoine, J.-M., Balmino, G., Loyer, S., Bruinsma, S., Perosanz, F., Marty, J.-C. & Gégout, P., 2005. *Three years of decadal geoid variations from GRACE and LAGEOS data*, CD-ROM, CNES/GRGS product (also on website: http://bgi.cnes.fr:8110/geoid-variations/README.html)

Carrere, L. & Lyard, F., 2003. Modelling the barotropic response of the global ocean to atmospheric wind and pressure forcing – comparisons with observations, *Geophys. Res. Lett.*, **30**(6), 1275, doi:10.1029/2002GL016473.

Chambodut, A., Panet, I., Mandea, M., Diament, M., Holschneider, M. & Jamet O., 2005. Wavelet frames: an alternative to spherical harmonic representation of potential fields, *Geophys. J. Int.*, **3,** 875–899, doi:10.1111/j.1365-246X.2005.02754.x.

Curray, J., 2005. Tectonics and history of the Andaman Sea region, *J. Asian Earth Sci.*, **25,** 187–232.

Dickey, J. *et al.*, 1997. *Satellite gravity and the geosphere*. National Research Council Report, Nat. Acad. Press, Washington, DC.

Dziewonski, A.M. & Anderson, D.L., 1981. Preliminary reference earth model (PREM), *Phys. Earth Planet. Inter.*, **25,** 297–356.

Galahaut, V.K., Nagarajan, B., Catherine, J.K. & Kumar, S., 2006. Constraints on 2004 Sumatra-Andaman earthquake rupture from GPS measurements in Andaman-Nicobar islands, *Earth Planet. Sci. Lett.*, **242,** 365–374.

Gross, R. & Chao, B., 2001. The gravitational signature of earthquakes, in *Gravity, Geoid and Geodynamics 2000*, IAG Symposia, Vol.123, pp. 205–210, Springer-Verlag, New-York.

Han, S.-C., Shum, C.K., Bevis, M., Ji, C. & Kuo, C.-Y., 2006. Crustal dilatation observed by GRACE after the 2004 Sumatra-Andaman earthquake, *Science*, **313,** 658–662.

Hashimoto, M., Choosakul, N., Hashizume, M., Takemoto, S., Takiguchi, H., Fukuda, Y. & Fujimori, K., 2006. Crustal deformations associated with the great Sumatra-Andaman earthquake deduced from continuous GPS observation, *Earth, Planets, Space*, **58,** 127–139.

Holschneider, M., 1995. *Wavelets: An Analysis Tool*, Oxford Sciences Publications, Oxford.

Holschneider, M., Chambodut, A. & Mandea, M., 2003. From global to regional analysis of the magnetic field on the sphere using wavelet frames, *Phys. Earth Planet. Inter.*, **135,** 107–124.

Hu, Y., Wang, K., He, J., Klotz, J. & Khazaradze, G., 2004. Three-dimensional viscoelastic finite element model for post-seismic deformation of the great 1960 Chile earthquake, *J. Geophys. Res.*, **109,** B12403, doi:10.1029/2004JB003163.

Ivins, E.R., 1996. Transient creep of a composite lower crust 2. A polymineralic basis for rapidly evolving postseismic deformation modes, *J. Geophys. Res.*, **101**(B12), 20 005–20 028.

Karato, S.-I. & Wu, P., 1993. Rheology of the upper mantle: a synthesis, *Science*, **260,** 771–778.

Khan, P.K. & Chakraborty, P.P., 2005. Two-phase opening of Andaman Sea: a new seismotectonic insight, *Earth Planet. Sci. Lett.*, **229,** 259–271.

Lay, T. *et al.*, 2005. The great Sumatra-Andaman earthquake of 26 december 2004, *Science*, **308,** 1127–1133.

Lemoine, J.-M., Bruinsma, S., Loyer, S., Biancale, R., Marty, J.-C., Perosanz, F. & Balmino, G., 2007. Static and temporal gravity field models inferred from GRACE data, *Adv. Space Res.*, in press.

Masterlark, T., DeMets, C., Wang, H.F., Stock, J. & Sanchez, O., 2001. Homogeneous vs heterogeneous subduction zone models: co-seismic and post-seismic deformation, *Geophys. Res. Lett.*, **28,** 4047–4050.

Mikhailov, V., Tikhostky, S., Diament, M., Panet, I. & Ballu, V., 2004. Can tectonic processes be recovered from new satellite gravity data? *Earth Planet. Sci. Lett.*, **238,** 281–297.

Minster, J.B. & Anderson, D.L., 1981. A model of dislocation-controlled rheology for the mantle, *Philos. Trans. R. Soc. Lond.*, **299,** 319–356.

Mishra, O.P., Kayal, J.R., Chakraborty, G.K., Singh, S. & Ghosh, D., 2007. Aftershock investigation in the Andaman-Nicobar islands of India and its seismotectonic implications, *Bull. Seismol. Soc. Am.*, **97**(1A), S71–S85.

Panet, I., Chambodut, A., Diament, M., Holschneider, M. & Jamet, O., 2006. New insights on intra-plate volcanism in French Polynesia from wavelet analysis of GRACE, CHAMP and sea-surface data, *J. Geophys. Res.*, **111**(B9), B09403, doi:10.1029/ 2005JB004141.

Pollitz, F., 1996. Co-seismic deformation from earthquake faulting on a layered spherical Earth, *Geophys. J. Int.*, **125,** 1–14.

Pollitz, F., Bürgmann, R. & Romanowicz, B., 1998. Viscosity of oceanic asthenosphere inferred from remote triggering of earthquakes, *Science*, **280,** 1245–1249.

Pollitz, F., Wicks, C. & Thatcher, W., 2001. Mantle flow beneath a continental strike-slip fault: post-seismic deformation after the 1999 Hector Mine earthquake, *Science*, **293,** 1814–1818.

Pollitz, F., 2003. Transient rheology of the uppermost mantle beneath the Mojave Desert, California, *Earth Planet. Sci. Lett.*, **215,** 89–104.

Pollitz, F., Banerjee, P. & Burgmann, R., 2006. Post-seismic relaxation following the great 2004 Sumatra-Andaman earthquake on a compressible self-gravitating Earth, *Geophys. J. Int.*, **167,** 397–420.

Subarya, C. *et al.*, 2006. Plate-boundary deformation associated with the great Sumatra-Andaman earthquake, *Nature*, **440,** 46–51, doi:10.1038/nature04522.

Sun, W. & Okubo, S., 2004. Coseismic deformations detectable by satellite gravity missions: a case study of Alaska (1964, 2002) and Hokkaido (2003) earthquakes in the spectral domain, *J. Geophys. Res.*, **109,** B04405.

Vigny, C. *et al.*, 2005. Insights into the 2004 Sumatra-Andaman earthquake from GPS measurements in southeast Asia, *Nature*, **436,** 201–206.

Wahr, J., Molenaar, M. & Bryan, F., 1998. Time variability of the Earth's gravity field: hydrological and oceanic effects and their possible detection using GRACE, *J. geophys. Res.*, **103,** 30 205–30 229.

Wessel, P. & Smith, W.H.F., 1995. New version of the Generic Mapping Tool released, *Eos Trans. AGU*, **76,** 329.

APPENDIX A

Let us consider a Cartesian coordinates frame with *Oz* the vertical axis, and a lithospheric plate of uniform thickness parallel to the *xOy* plane. For the sake of simplicity, we assume that the lithospheric plate is a thin plate of infinite dimension in the *Oy* direction. A uniform extensional force P parallel to the *Ox* axis is applied to its end (Fig. A1).

The total length of the plate in the x direction is L. The plate is made of three blocks B_1, B_2 and B_3 of respective lengths L_1, L_2 and L_3 in the x direction, so that $L = L_1 + L_2 + L_3$. Considering the structure of the Andaman Sea, we choose $L_1 = L_2 = L_3 = 200$ km. The Poisson ratio υ is constant in each block and the Young modulus E_2 of block B_2 is a times smaller than its value E in the other blocks: $E_2 = E/a$. Based on the tectonic history of the Andaman Sea, part of the Andaman Sea lithosphere is indeed likely to be more compliant.

Thus, we are dealing with a plane stress problem:

$$\varepsilon_y = 0 \tag{A1}$$

$$\sigma_z = 0, \tag{A2}$$

and Hook's equations yields:

$$\varepsilon_x = (\sigma_x - \upsilon\sigma_y)/E \tag{A3.1}$$

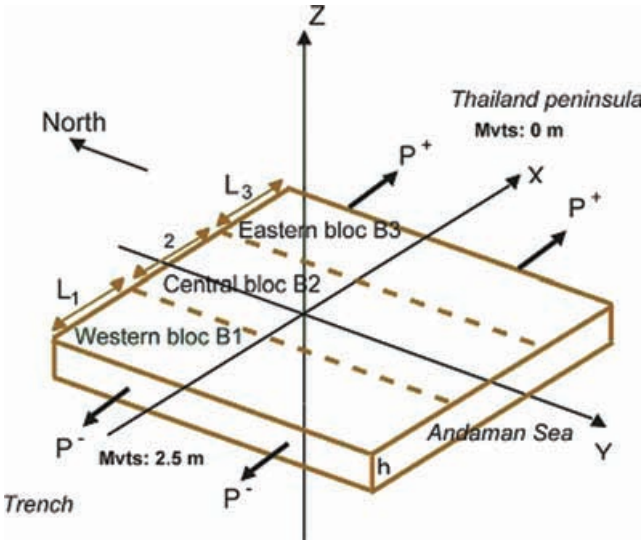

Figure A1. The block model of the lithosphere in the Andaman Sea. The Central Block corresponds to the basin affected by the first stage of ocean opening aborted 4 Myr ago (Khan & Chakraborty 2005), around longitude 97°E and latitude 7°N.

$$\varepsilon_y = (-\upsilon\sigma_x + \sigma_y)/E = 0 \tag{A3.2}$$

$$\varepsilon_z = (-\upsilon\sigma_x - \upsilon\sigma_y)/E. \tag{A3.3}$$

From eq. (A3.2) we get: $\sigma_y = \nu\sigma_x$, and from eqs (A3.1) and (A3.3):

$$\varepsilon_x = \sigma_x(1 - \upsilon^2)/E, \tag{A4}$$

and

$$\varepsilon_z = -\varepsilon_x\upsilon/(1 - \upsilon). \tag{A5}$$

The force P and the stress σ_x are constant along the directions *Ox* and *Oy*: $P = \sigma_x h = \text{const}$. The total shortening along direction *Ox* is given by:

$$\begin{aligned}\Delta L &= \Delta L_1 + \Delta L_2 + \Delta L_3 = \sigma_x(1 - \upsilon^2)(L_1 + aL_2 + L_3)/E \\ &= \sigma_x(1 - \upsilon^2)(L + (a - 1)L_2)/E.\end{aligned} \tag{A6}$$

The vertical displacement of the top of blocks 1 and 3 is given by:

$$\Delta h_{1,3} = \varepsilon_z h = -\Delta L h\nu/[(1 - \nu)(L + (a - 1)L_2], \tag{A7.1}$$

and for block 2 we derive:

$$\Delta h_2 = a\Delta h_{1,3}. \tag{A7.2}$$

The excess uplift (and subsequent subsidence) of block 2 is then:

$$\delta h = -(a - 1)\Delta L h\upsilon/[(1 - \upsilon)(L + (a - 1)L_2)]. \tag{A7.3}$$

Let us now estimate the change of the vertical load for the most compliant block (block B_2, standing for the Eastern and Mergui basin), assuming that density and thickness of the lithosphere was initially constant in the block but then changed during the extension process. For that, let us consider an elementary volume of unit length along the *Oy* direction, with height h and length l along the *Ox* direction. The variation of the load is given by:

$$\partial(\rho h) = \partial(\rho h l/l) = \partial(\rho h l)/l - \rho h l \partial l/l^2. \tag{A8}$$

The first term $\partial(\rho h l)$is the mass variation of the lithospheric plate. It is equal to zero. In the second term, we have: $\partial\, l/l = \varepsilon_x$. Using

eq. (A5) and taking into account the following relation: $\varepsilon_z = \Delta h/h$, yields:

$$\partial(\rho h) = \rho \Delta h(1-\upsilon)/\upsilon. \quad \text{(A9)}$$

The displacement of the density interface between water and rocks in result of subsidence produces a load variation, so the total variation is:

$$\begin{aligned}\partial_{wf}(\rho h) &= \rho \Delta h(1-\upsilon)/\upsilon - \rho_w \Delta h \\ &= \Delta h[(\rho - \rho_w) + \rho(1-2\upsilon)/\upsilon]. \quad \text{(A10)}\end{aligned}$$

The second term in eq. (A10) corresponds to the effect of dilatation. For an uncompressible media ($\upsilon = 0.5$), this term is equal to zero and the load variation is caused by subsidence only. Finally, the excess load in block B_2 is computed using eq. (A10) and substituting ∂h from eq. (A7.3) for Δh.

Let us now give a quantitative estimate for this load. We choose realistic values for the different parameters: $\Delta h = 2.5$ m (see Section 4), $h = 50$ km, $L = 600$ km, $L_2 = 200$ km, $\upsilon = 0.25$, $\rho = 2.7\ 10^3$ kg m^{-3} and $a = 1.5$. Eq. (A7.3) yields: $\partial h = 0.03$ m. Substituting this value into eq. (A10) yields: $\partial_{wf}(\rho h) = 213$ kg m^{-2}. This is equivalent to 15 cm of subsidence. If we choose: $L = 400$ km, then $\partial h = 0.17$ m and $\partial_{wf}(\rho h) = 300$ kg m^{-2} or 18 cm of subsidence.

Estimates of $\partial_{wf}(\rho h)$ only slightly depend on the value of Poisson ratio. Indeed, for increasing values of the Poisson ration, the second term in eq. (A10) vanishes but this is compensated by the fact that ∂h becomes three times larger, because of the multiplier $\upsilon/(1-\upsilon)$.